



# Depth-resolved chemical mapping of rock coatings using Laser-Induced Breakdown Spectroscopy: Implications for geochemical investigations on Mars



C. Lefebvre <sup>a,\*<sup>1</sup></sup>, A. Catalá-Espí <sup>b</sup>, P. Sobron <sup>a,2</sup>, A. Koujelev <sup>a</sup>, R. Léveillé <sup>a,3</sup>

<sup>a</sup> Space Science and Technology, Canadian Space Agency, 6767, route de l'aéroport, Saint-Hubert, Canada J3Y 8Y9

<sup>b</sup> Unidad Asociada UVa-CSIC, Avd. Francisco Vallés, Parque Tecnológico de Boecillo, E-47151 Boecillo, Valladolid, Spain

## ARTICLE INFO

### Article history:

Received 5 December 2013

Received in revised form

4 April 2016

Accepted 5 April 2016

Available online 13 April 2016

### Keywords:

Mars

Laser-Induced Breakdown Spectroscopy

Rock coatings

Depth profiling

Svalbard

## ABSTRACT

We demonstrate that Laser-Induced Breakdown Spectroscopy (LIBS) is capable of identifying the presence of natural rock coatings, and we define LIBS signatures of complex multi-layered coatings. This is illustrated by detailed LIBS analysis, in Mars-simulated conditions, of a rock collected in the Svalbard Islands, and which is analogous to some altered Martian rocks. The sample is a basaltic rock with sub-mm Ca–Mg–Fe–Si rich mineral coatings. LIBS elemental analysis of several distinct regions on the surface of the rock demonstrates the variability of chemical compositions of the various coatings, which is confirmed by complementary scanning electron microscope (SEM) analysis. Furthermore, the LIBS analysis as a function of the depth at different locations shows chemical variability, indicative of penetration through thin coatings of varying composition. Fine-scale, three-dimensional LIBS analysis is of interest for identifying and characterizing coatings on martian rocks, likely originating from aqueous processes, providing a rapid chemical composition as a function of the layers and further understanding of the formation of the deposits and on planetary evolution.

Crown Copyright © 2016 Published by Elsevier Ltd. All rights reserved.

## 1. Introduction

Laser-Induced Breakdown Spectroscopy (LIBS) is an emerging chemical analysis technique for studying a wide range of natural and synthetic materials. In LIBS, each short, high-energy laser pulse, focused onto a target, ablates a small amount of material. The laser-induced plasma emission provides information about the elemental composition of the target. By using multiple laser shots at a given location, the laser can effectively drill down into a sample and generate plasmas at increasingly greater depths with each successive shot, providing information on the chemical composition as a function of depth. The rate of penetration, i.e. the amount of ablated material, with each laser shot is dependent on laser (e.g., power, beam diameter, pulse rate) and target (e.g.,

density, hardness, cohesiveness) characteristics. Thus, LIBS is particularly well suited for investigating surface coatings on solid materials and performing chemical depth-profiles. LIBS has been used for investigating layers and performing depth profiles in numerous industrial, pharmaceutical and cultural heritage applications (Vadillo and Laserna, 1997; St-Onge and Sabsabi, 2000; Balzer et al., 2005; Novotný et al., 2007; Kim et al., 2007; Madamba et al., 2007; Alvira et al., 2009; Cabalín et al., 2011; Dubey et al., 2012). However, its use in investigating complex, geological coatings has been limited so far. Preliminary work has shown that LIBS can provide qualitative compositional information on natural coatings on rocks (cf. Wiens et al., 2004; Sharma et al., 2007; Lanza et al. 2012). In addition, pre-flight laboratory tests, measurements with engineering models, and in situ analyses of actual martian rocks also suggest that the LIBS instrument that is included in the ChemCam package on the Mars Science Laboratory (MSL) Curiosity rover is able to identify and characterize rock coatings on Mars and perform depth profiles through multiple coatings (Wiens et al., 2012; Cousin, 2012; Blaney et al., 2013; Lanza et al., 2013; Léveillé et al., 2014; Lanza et al., 2015). However, LIBS analyses of natural rock coatings have been limited in their scope, and few studies provide complementary analytical data acquired in controlled laboratory conditions. Preliminary results suggest that the interpretation of LIBS data from complex natural

\* Corresponding author.

E-mail addresses: [catherine.lefebvre@emt.inrs.ca](mailto:catherine.lefebvre@emt.inrs.ca) (C. Lefebvre), [richard.leveille@mcgill.ca](mailto:richard.leveille@mcgill.ca) (R. Léveillé).

<sup>1</sup> Present address: INRS-EMT, 1650 Boulevard Lionel-Boulet, Varennes, Canada J3X 1S2.

<sup>2</sup> Present address: SETI Institute, 189 Bernardo Ave #100, Mountain View, CA 94043, USA and Malauva Labs, 822 Allen Ave #A, St. Louis, MO 63104, USA.

<sup>3</sup> Present address: McGill University, 3450 University Street, Montreal, Canada H3A 0E8.

geological materials is not straightforward due to a complex interplay of sample heterogeneities and laser-matter interaction. Clearly, it is important to advance LIBS investigations of depth profiling for complex natural rock samples in the context of planetary exploration.

On Earth, natural rocks are commonly found with coatings, which include rock varnish and various secondary mineral deposits, and with alteration rinds. Desert rock coatings are particularly diverse and form as a result of a complex interplay of chemical, physical and biological processes (Dorn, 1998). Also, alteration rinds may also develop by oxidative weathering in systems with little liquid water, such as in the hyper-arid and hypo-thermal Beacon Valley, Antarctica (Salvatore et al., 2013). All of these may record evidence of past aqueous activity, in particular fluid chemical composition, pH and temperature. On Mars, sub-millimeter veneers, thicker weathering rinds and depositional coatings have been identified on rocks by a combination of measurements made by the Mars Exploration Rovers (MER) *Opportunity* and *Spirit* as well as the *Curiosity* rover (McSween et al., 2006; Knoll et al., 2008; Mahaney et al., 2012; Lanza et al., 2015). Remote-sensing observations have also led to the suggestion of widespread alteration features, including alteration rinds and coatings (e.g., Bishop et al., 2002; Michalski et al., 2006). These features all provide important information and constraints on the nature, timing, and duration of aqueous alteration on Mars. However, rock coatings, even those as thin as a few micrometers, can significantly alter the surface appearance of rocks, thus complicating passive remote-sensing measurements and in situ chemical and mineralogical measurements made by rovers. While detailed examinations of coatings have been done by combining the use of the Alpha Particle X-ray Spectrometer (APXS) and the rock abrasion tool on the MER rovers (e.g., Haskin et al., 2005), this approach is time-consuming, is limited in spatial resolution, and requires the rover to be positioned close to the target.

In this work, we have performed a three-dimensional semi-quantitative investigation of the chemical variability in multi-layered, alteration coatings on a natural rock sample. In previous work, Sobron et al. (2013) demonstrated how LIBS could be used for rapid semi-quantitative characterization of different rock layers at the outcrop scale. Here we focus instead on sub-millimeter thick natural mineral coatings. We demonstrate that LIBS can be used to identify the presence of coatings in complex geological samples and we explore the concept of a LIBS coating signature as a tool for

geochemical analysis. Data processing based on the elemental intensity ratios also provides three-dimensional data on the chemical variability within multi-layer coatings. The chemical variation trends are confirmed by complementary scanning electron microscopy (SEM) analysis. Rock coatings record multiple episodes of aqueous activity and they track fluid evolution over time, thus indicating local or regional environmental changes. Our findings can contribute to a better understanding of fine-scale three-dimensional chemical analyses by LIBS of complex geological targets in landed planetary exploration missions (e.g., Léveillé et al., 2014). Such analyses can provide information on the detailed chemical composition of fine-scale features (e.g. coatings, alteration rinds, veins, cements), thus providing critical information on habitability and planetary evolution.

## 2. Methodology

### 2.1. Instrumentation

The LIBS setup, depicted in Fig. 1, uses a commercial Q-switch Nd:YAG laser (LPY150, Lambda Physik, Germany) generating 8 ns pulses at 1064 nm at a repetition rate of 1 Hz with pulse energy of 16 mJ. The laser pulses pass through a pierced lens, then through the viewport of the chamber and are focused by a focusing lens ( $L_2, f=75$  mm) onto the target placed inside the chamber. The emission from the plasma is collected by the latter lens, collimated, focused by the pierced lens ( $L_1, f=75$  mm) onto the optical fiber, and transported to the spectrometer (Ocean Optics, HR2000, USA). A seven-channel spectrometer is used, consisting of seven spectrometers attached to a demultiplexer. The spectral range covers from 200 to 900 nm with a resolution of 0.1 nm. The delay between emission and acquisition and integration times are  $t_d=1\ \mu s$  and  $t_b=2\ ms$ , respectively. This coaxial geometry has the advantage of being compact for potential field applications. The chamber (shown in Fig. 1(b)) is filled with  $\text{CO}_2$  gas and the pressure is kept at 6.6 mbar to simulate Mars' atmosphere. The chamber sits on a XY translation stage, which allows the chamber to move and to probe different spots on the sample. The experiments were performed at room temperature.

Semi-quantitative elemental analyses of the same sample were performed with an Inspect F-50 scanning electron microscope (SEM; FEI, Hillsboro, OR) equipped with a TEAM energy dispersive

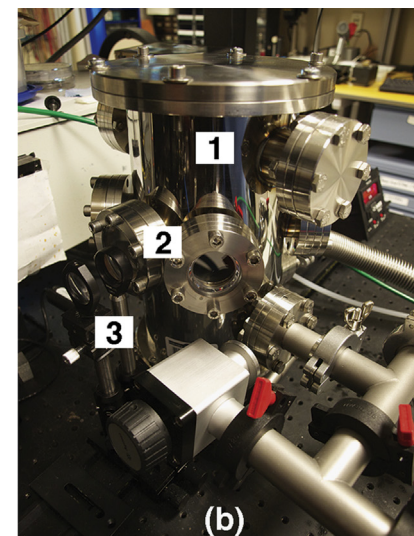
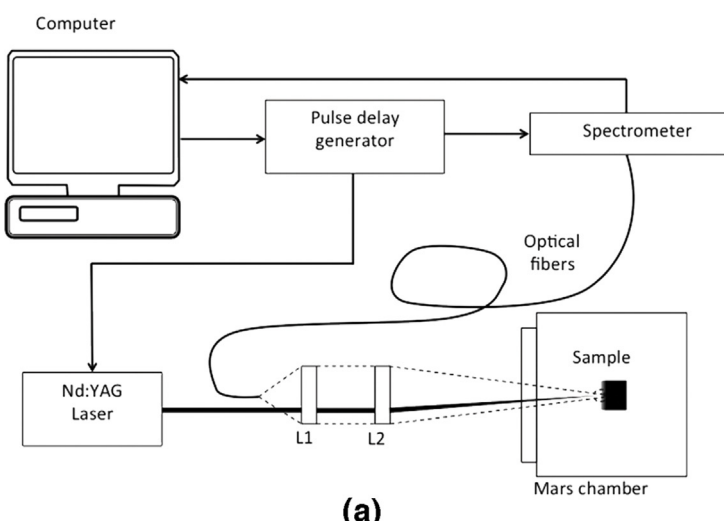


**Fig. 1.** (a) LIBS setup diagram and (b) Mars chamber and part of the optical path. Numbers 1, 2 and 3 correspond respectively to the Mars Chamber, the viewports for accessing the interior of the chamber, and the focusing and collection system.

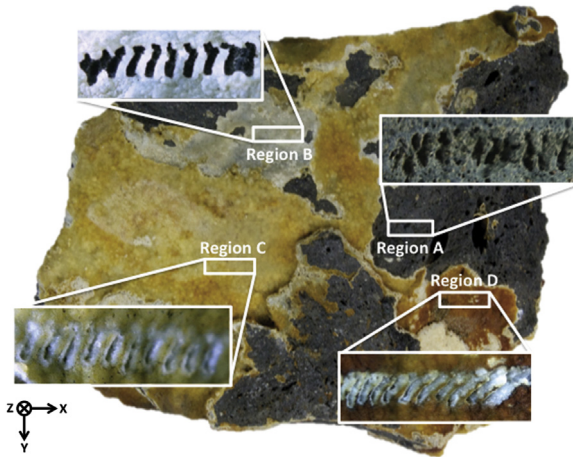


**Fig. 2.** Mineral-coated basaltic rock from Svalbard, with the four selected regions (A, B, C and D). A matrix of  $10 \times 10$  points were analyzed on each of the four regions, and the inset pictures depict the craters formed by the laser shots (50 at each point). (For interpretation of the references to color in this figure, the reader is referred to the web version of this article.)

(EDS) X-ray analysis system (EDAX, Mahwah, NJ). Small sub-samples of each of the main layers were carefully removed and placed on carbon tape on aluminum stubs. Analyses were performed on these uncoated sub-samples under high-vacuum with an accelerating voltage of 10 kV. Standardless quantification was performed using the Smart Quant software model. For each sample, 4–6 analysis spots were chosen, and the results were averaged.

## 2.2. Sample description

Rock sample AM11063 was collected during the NASA ASTEP-funded AMASE 2011 Expedition to the Svalbard Islands (Steele et al., 2011). It is a basaltic rock non-homogeneously covered with various sub-mm mineral coatings, as illustrated in Fig. 2. More details of the thickness and composition are discussed in the following section. The sampling site lies near the top of the Sverrefjell volcano, a unique alkali basaltic stratovolcano dominated by pyroclastics and with abundant mantle-derived xenoliths (Skjelkvåle et al., 1989; Treiman et al., 2002). The Sverrefjell volcanic complex erupted at  $\sim 1$  Ma, or more recently, and possibly beneath ice (Skjelkvåle et al., 1989; Treiman et al. 2002; Blake et al. 2011). Various Ca–Mg–Fe carbonate-rich deposits have been observed cementing basaltic breccias, coating the walls of vertical volcanic pipes, and as globules in basalts and in ultramafic xenoliths (Treiman et al., 2002; Blake et al., 2011). The globules, in particular, are believed to be the best terrestrial analogs to the carbonate globules in the Mars meteorite Allen Hills 84001 (i.e., ALH84001; Treiman et al., 2002). In addition, some of these carbonates are similar in composition to carbonates on Mars, such as those in the Comanche outcrop studied by the MER Spirit (Treiman et al., 2002; Morris et al., 2010). While the Comanche carbonates are thought to be of hydrothermal origin (Morris et al., 2010), both low-temperature and high-temperature processes have been invoked to explain both the ALH84001 carbonates as well as the carbonates found at Sverrefjell and neighboring volcanic complexes (Treiman et al., 2002; Morris et al., 2010; Amundsen et al., 2011; Niles et al., 2013).

## 2.3. Data collection and analysis

In this study, we investigated four visually-distinct regions of the AM11063 sample, identified in Fig. 2. Region A is a dark-colored, vesicular basalt showing no visible coating. It is the base

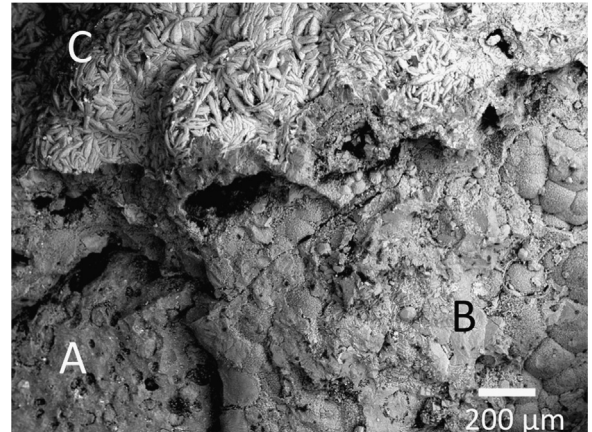


**Fig. 3.** SEM image Svalbard sample showing the four main layers. A is the basalt substrate, B is the light-toned, carbonate-rich layer, and C is the darker-toned, upper-most layer than is more rich in Si and Fe. Layer D is not seen in this view.

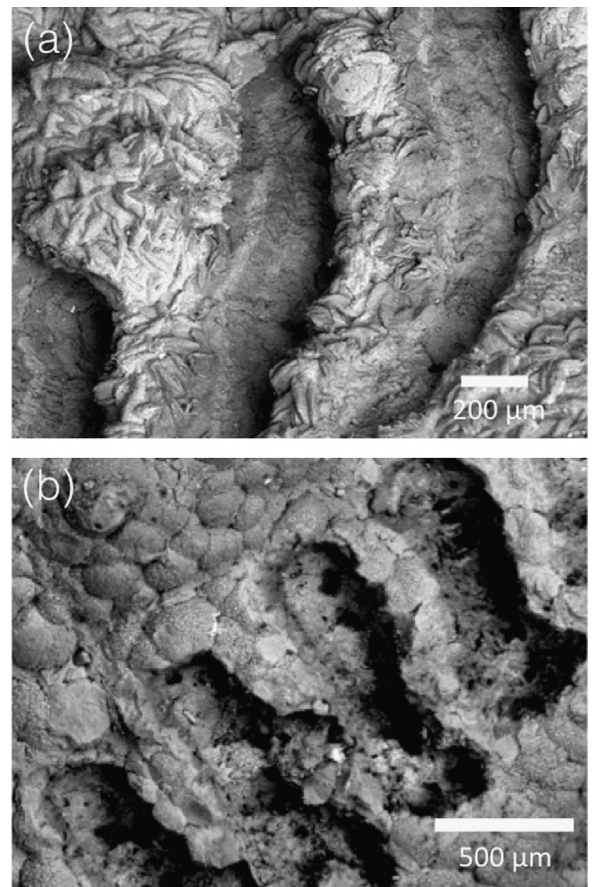


**Fig. 4.** Detailed backscattered electron SEM images showing the characteristics of the LIBS craters in two different layers: (a) rows of LIBS craters in layer D showing fine-scale variability in both texture and composition (note light-toned band in middle of the layer, as seen in the crater walls); (b) rows of LIBS craters in Layer B; the base of the craters shows the vesicles from the underlying basalt (layer A) substrate.

rock on which the coatings in all other regions are emplaced. Region B is a thin light-toned coating that appears to be directly coating the basalt. Regions C and D are thicker coatings with variable colors ranging from yellow-brown to reddish-brown. The four different layers also have distinct textures at the sub-mm scale as seen in SEM images (Figs. 3 and 4). The sequence of deposition of the coatings on the base rock is explored in detail with LIBS, and confirmed by SEM.

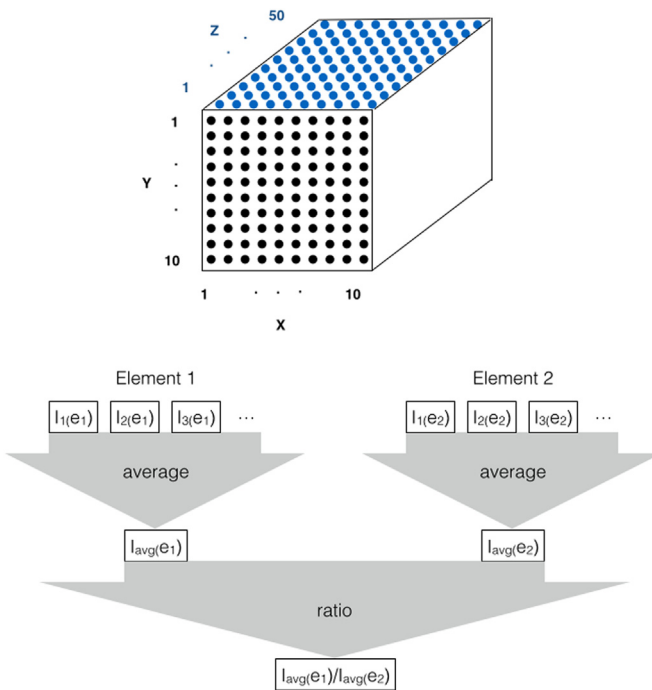


**Fig. 5.** (top) 3D map of LIBS sampling locations on a region of the sample. (bottom) Steps of the analysis of elemental lines and element ratios. For instance  $I_{1(e_1)}$  corresponds to the intensity of the atomic line 1 of the Element 1.

The steps of the LIBS analysis are depicted in Fig. 5. For each of the four regions, a matrix of  $X=10$  by  $Y=10$  points was analyzed (covering an estimated area of 2 mm $\times$ 6 mm, the step size being different in the X and Y direction). At each point, 50 laser shots are fired and the signal induced by each of the laser shots was recorded, obtaining a compositional profile into the rock surface (i.e. Z dimension). A total of 5000 spectra were therefore recorded in each region. Based on SEM, the depth of the craters has been estimated to be in the range of 200–300  $\mu$ m. Rather than evaluating the thickness of the coatings, it is the chemical change within this depth that is probed. Once the data collected, each single spectrum was normalized to its total intensity to correct for shot to shot fluctuations in laser energy output. This normalization was performed separately on each spectral range covered by the seven individual detectors.

At a first level of analysis, all elemental lines could be analyzed and compared amongst the various spectra, and also amongst the four regions. We selected four elements (Ca, Fe, Si, Mg) for further analysis, based on their LIBS signal strength variability amongst the regions and shot number as well as for their chemical relevance in alteration products expected to form from the alteration of basalt and (or) deposition from hydrothermal fluids. For specific elements, several lines have been selected according to the strength, lack of self-absorption and lack of overlapping lines (as listed in Table 1). Also, SEM analysis confirmed that these elements are the most important in concentration.

On a second level, a qualitative comparison was performed, following these steps:

- (1) For each element, the line intensity was evaluated. Line intensity is defined here as the total counts within full width at half maximum (FWHM) of the line. (Note that other definitions of line intensity, such as the area under the line, are also acceptable.)
- (2) All the line intensities of a given element were averaged together, giving one averaged intensity per element (Koujelev and Lui, 2011).
- (3) Elemental ratios were determined using the averaged element intensities. This qualitative analysis of the average

**Table 1**

LIBS atomic emission lines for the regions A, B, C, and D and the corresponding normalized line intensity. The gray zones are the selected lines of Ca, Mg, Fe and Si used for LIBS analysis.

Element	(nm)	Normalized line intensity			
		Region A	Region B	Region C	Region D
Al	308.242	0.00040	0.00022	0.00014	0.00014
Al	394.422	0.00099	0.00076	0.00034	0.00068
Al	396.169	0.00119	0.00082	0.00041	0.00062
C	247.912	0.00224	0.00212	0.00214	0.00229
C	833.683	0.00067	0.00059	0.00071	0.00059
C	909.664	0.00089	0.00067	0.00091	0.00066
Ca	317.960	0.00103	0.00237	0.00160	0.00227
Ca	422.719	0.00155	0.00160	0.00143	0.00176
Ca	643.901	0.00307	0.00526	0.00402	0.00559
Ca	644.955	0.00115	0.00217	0.00155	0.00241
Ca	645.509	0.00074	0.00102	0.00086	0.00111
Ca	646.227	0.00255	0.00456	0.00341	0.00489
Ca	849.917	0.00166	0.00264	0.00204	0.00273
Ca	854.202	0.00371	0.00655	0.00536	0.00645
Ca	866.356	0.00439	0.00725	0.00622	0.00743
Fe	356.528	0.00043	0.00032	0.00041	0.00036
Fe	361.912	0.00064	0.00041	0.00058	0.00049
Fe	363.184	0.00067	0.00061	0.00066	0.00067
Fe	372.761	0.00050	0.00054	0.00056	0.00058
Fe	532.797	0.00070	0.00051	0.00073	0.00060
H	656.337	0.00083	0.00077	0.00084	0.00075
K	766.576	0.00549	0.00335	0.00084	0.00070
K	769.900	0.00409	0.00290	0.00080	0.00061
Li	611.031	0.00042	0.00072	0.00059	0.00076
Li	670.761	0.00128	0.00116	0.00099	0.00084
Mg	285.606	0.00135	0.00197	0.00271	0.00205
Mg	880.735	0.00046	0.00069	0.00075	0.00074
Na	819.586	0.00395	0.00113	0.00060	0.00052
O	777.729	0.00410	0.00339	0.00548	0.00360
Si	288.561	0.00117	0.00086	0.00028	0.00035
Ti	334.944	0.00331	0.00093	0.00038	0.00040
Ti	336.160	0.00252	0.00078	0.00037	0.00039
Ti	453.555	0.00215	0.00101	0.00083	0.00076
Ti	498.494	0.00064	0.00033	0.00022	0.00020
Ti	499.423	0.00056	0.00034	0.00016	0.00038
Ti	501.043	0.00039	0.00030	0.00029	0.00026
Ti	625.768	0.00089	0.00071	0.00060	0.00070
Ti	626.060	0.00072	0.00066	0.00060	0.00067

intensity ratios was done both over the region (averaged over all sampling locations, Fig. 8) and over a line of a region ( $Y=2$ , Fig. 9).

### 3. Discussion

#### 3.1. SEM analysis

The semi-quantitative analysis of the composition (in oxide wt%) of the four regions by SEM-EDS is detailed in Table 2. Quantifiable concentrations of Al, Mg, Fe, Si, Na, K, Ca and S have been detected. The estimated concentrations vary from one region to the other. Region A (base rock) has a largest concentration of Si and Al, as well as substantial Mg, Fe and Ca. It also has the highest analysis total, which is indicative of less volatiles present. These characteristics are consistent with a basaltic composition. Region B has the highest concentration in Ca and Mg. Region C and D have similar large concentrations in Si and Mg. In comparison to region C, region D has a larger concentration in Al and Fe. From the elements detected, Al, Mg, Ca, Fe, Si are those that are the most abundant and these vary in concentration from one region to another. We also observed variability in composition within a given layer (possible ‘sub-layers’; chemical data not shown; c.f. Fig. 4) as well as the presence of possible cements and unidentified

inclusions. Together, these characteristics further contribute to the complex nature of the sample.

### 3.2. Three-dimensional LIBS analysis

The bulk LIBS spectra, resulting from averaging over all the sampling locations and by depth in each location, are shown in Fig. 6 for each of the four selected regions on the sample. Several elements can be identified in these spectra. Most of these elements are gathered in Table 1 showing a qualitative comparison of the normalized intensity over the four regions. Note that the laser interaction efficiency differs from one element to another. Therefore the absolute elemental intensity should not be directly translated into elemental concentration. We base our discussion here on the elemental intensities and intensity ratios. It should be noted, however, that LIBS can also be used to perform quantitative

analysis by using univariate or multivariate data analysis methods to extract the elemental concentration (Ciucci et al., 1999; Sirven et al., 2007; Doucet et al., 2007; Clegg et al., 2009; Koujelev and Lui, 2011), though this is beyond the scope of our current study. From Fig. 4 and Table 1, one can observe that the line intensity of some elements vary from one region to another. Furthermore, only specific elements show an important variability of the line intensities as a function of the depth and as a function of the four regions probed. Also, the SEM analysis also demonstrates that these same major elements show a variation in concentration between the four regions. Therefore, we choose to concentrate on four major cations: Ca, Mg, Fe and Si. They are present in each region analyzed and are some of the most relevant for tracking chemical changes in depth and amongst the selected regions (see below).

A closer look at selected lines of the major elements shows that there are line intensity variations with depth as a function of the laser shots (spectrum averaged over all sampling locations), as illustrated in Fig. 7 for the 1st, 7th, 12th, 25th and 50th laser shots. In general, the line intensity decreases with the laser shot number. This variation is due to the fact that the plasma efficiency translated by the total emission signal generally decreases with depth (Noll, 2012). However some lines do not follow the same general trend as a function of depth. For instance, Ca (643.90 nm) in region C and D, as well as Fe (361.91 nm) in region B do increase in intensity as the laser shot number increases. We also verified that the total intensity is relatively stable, and it does not follow the same trend as a given atomic line intensity, such that the variation is unlikely to be due to the laser pulse energy fluctuation. This is indicative of a chemical change within a specific region. This is qualitatively consistent with observations by Lanza et al. (2012, 2015) for LIBS analyses of natural rock varnish. The question of how this chemical change evolves across the selected coating regions, and whether we can define a clear signature of coatings by analyzing the signal as a function of laser shots within a single region is addressed by looking in the recorded LIBS spectra at the averaged line intensity ratios as a function of depth.

We focus our analysis on Ca, Mg, Si, and Fe (note that O is detected, as is common for silicates, oxides, carbonates, or sulfates,

**Table 2**  
Average elemental concentrations (4–6 locations per coating) in coatings based on SEM-EDS analyses.

Average elemental concentration (oxide wt%)				
	Region A	Region B	Region C	Region D
Al <sub>2</sub> O <sub>3</sub>	11.7	0.7	5.6	8.9
MgO	15.8	20.9	18.7	16.0
FeO	5.8	2.5	10.4	9.8
SiO <sub>2</sub>	42.1	3.4	32.6	33.1
NaO	1.8	–	0.1	–
K <sub>2</sub> O	1.5	–	0.68	2.2
CaO	6.3	27.3	3.5	4.00
SO <sub>3</sub>	5.5	0.6	0.4	2.7
Total	78.8	54.7	66.12	67.7
Average elemental ratios (wt%)				
Ca/Fe	0.99	10.02	0.31	0.37
Mg/Fe	2.10	6.46	1.40	1.26
Si/Fe	4.36	0.82	1.89	2.03

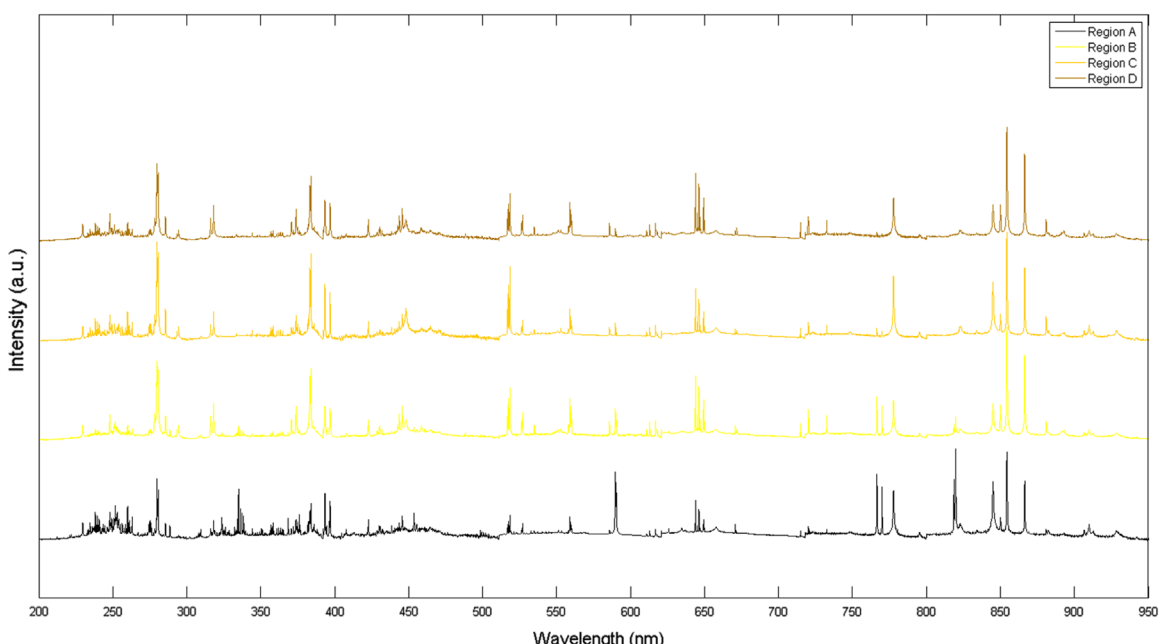


**Fig. 6.** Total bulk LIBS spectra, normalized to the total intensity, of the four regions A, B, C and D of the Svalbard rock. The represented spectra were averaged over the 50 laser shots and over all sampling locations, for each individual region.

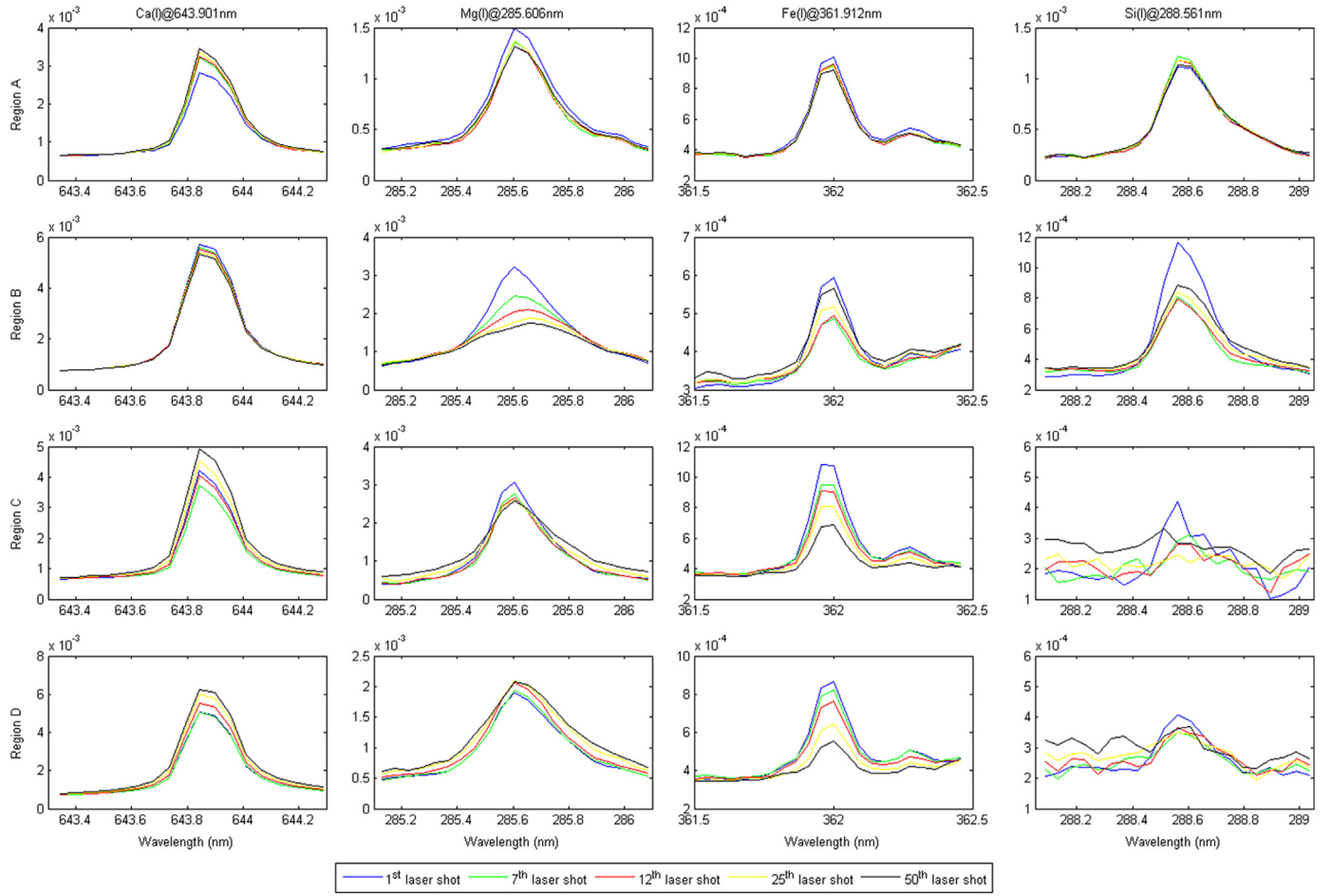


**Fig. 7.** Close-up view of selected lines, normalized to the total intensity and averaged over all sampling locations, for Ca I (643.90 nm), Mg I (285.61 nm), Fe I (361.91 nm) and Si I (288.56 nm), showing the variability in the LIBS line intensity for the 1st, 7th, 12th, 25th and 50th laser shots for each of the four regions (A, B, C and D) of the Svalbard rock.

but is not discussed here for simplicity), which all show varying proportions and distinct trends both in LIBS and SEM-EDS measurements. Fe shows the least variability as a function of depth in region A, which is the base rock. Consequently, Fe should show the most constant concentration with depth (assuming a relatively homogeneous bulk rock composition). It is thus a good candidate for the ratio analysis. The ratios (Ca/Fe, Mg/Fe, Si/Fe) is discussed in details below. The intensity ratio as function of the laser shot number, averaged over all sampling locations, is illustrated in Fig. 8. The lateral and depth variation of the ratio (along a line  $Y=2$ ) is illustrated as a contour plot in Fig. 9. For comparison, Table 2 also provides the elemental ratios Ca/Fe, Mg/Fe and Si/Fe from the SEM-EDS analysis. It is important to mention that these ratios are only for qualitative comparison and can hardly be used for assessing the accuracy of LIBS results, which is not the focus of our study, since the methodology, the sampling and the statistics are different. The interest of the comparison of the two methods and the focus of this study is to show the evolution of the chemical composition among the four selected regions. From SEM and LIBS data, it is clear that region A is relatively enriched in Si, that region B is relatively enriched in Ca and Mg, and that regions C and D have a similar chemical composition with respect to Ca, Mg, Si and Fe. Moreover, this study aims to show the 3D chemical variability at a given region (i.e. variation as function of the depth). We do not provide this information in the oxide wt% nor in the elemental ratios from the SEM analysis because it was performed only at the surface of each region. However, the 3D variability in the texture can definitely be appreciated visually from the SEM

pictures (see Fig. 4). Visible inspection and SEM imagery are consistent with region A being basalt, region B being a light-toned material and regions C and D being of similar, darker-toned material.

In general, from the LIBS signal, region A shows the least amount of variability as function of the depth, with the lowest Mg/Fe, Ca/Fe and Si/Fe ratios. Region B contains the highest intensities of Ca/Fe and Mg/Fe relative to regions A, C, and D. Regions C and D show a higher Si/Fe relative to regions A and B. Note that there exist significant differences in each region and they are described below.

Region A shows significantly less variability in relative intensities of Ca, Mg, Fe, and Si as a function of laser shot than the other regions because it has no coating. This is corroborated by the SEM data. Region A also shows a distinct overall composition, namely the lowest and most constant Ca/Fe, Mg/Fe and Si/Fe intensity ratios. The color and texture displayed in Fig. 2 suggest that region A is composed of one single material, which is interpreted to be basalt, and this is also consistent with the observed uniform composition.

In region B, the Ca/Fe and Mg/Fe relative intensities are both high near the surface, but decrease as a function of depth. Interestingly, the Si/Fe ratio approaches that of region A. These findings are consistent with region B consisting of a coating dominated by Ca- and Mg-carbonates and with no abundant Fe-bearing phase. This white-colored layer sits on top of the basaltic substrate, which is region A. It is therefore possible that the laser drilled through the coating of region B into the underlying region A (Fig. 2).

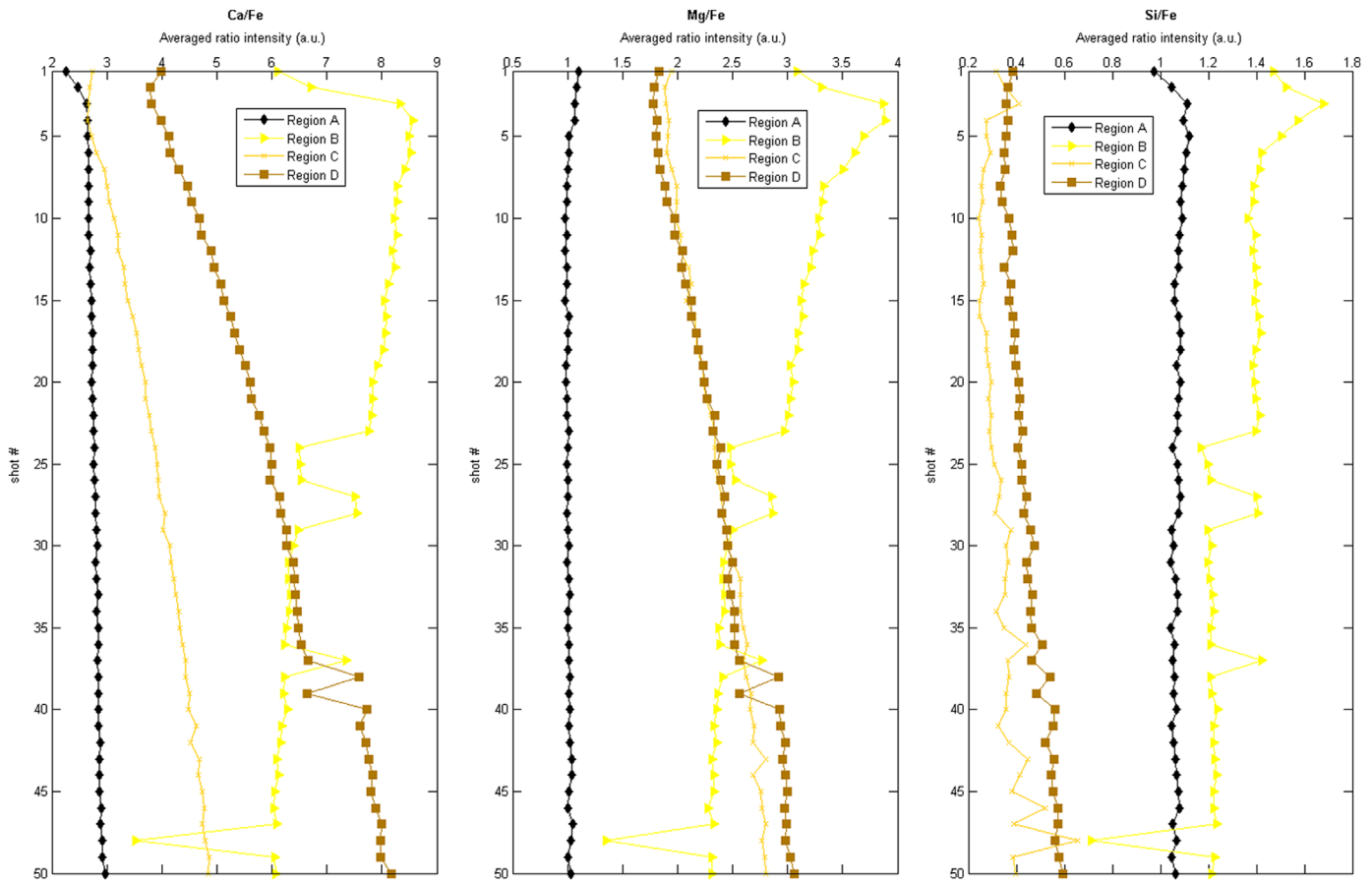


**Fig. 8.** Elemental ratios (Ca/Fe, Mg/Fe, Si/Fe) as a function of laser shot number of the four regions (A, B, C, D). The elemental ratio is obtained by normalization of the main element averaged intensity to the Fe averaged intensity, averaged over all sampling locations of each region.

Thus, the spectra from the deepest parts (highest number of laser shots) may show contributions from both regions B and A. Indeed, SEM observations show that this is most likely to have occurred (Fig. 4).

Regions C and D share several compositional similarities and appear to be closely related; they also show similar textures as seen in SEM observations. In these two regions, the relative intensity of Ca/Fe and Mg/Fe increases as a function of laser shot, while the relative intensity of Si/Fe decreases slowly. The strong anti-correlation between the relative intensities of Ca+Mg and Fe+Si is a clear indication of major changes in the chemical composition as a function of the laser shot number. We interpret these results to indicate the presence of a layered structure for regions C and D featuring an upper layer rich in Fe and Si, and a lower layer rich in Ca and Mg. No sharp transition boundary is evident between the Fe-Si-rich upper layer, and the Ca-Mg-rich lower layer, which suggests that these two layers have heterogeneous boundaries (also see further discussion below), as would be expected for natural mineral deposits. The Fe-enrichment is most likely due to the presence of iron oxy/hydroxides consistent with the red-orange color of the surface of the coating (Fig. 2). The Si is likely found in iron oxy/hydroxides or possibly as a distinct  $\text{SiO}_2$  phase. The enrichment in Ca and Mg in the lower layers of regions C and D is most likely attributed to Ca- and Mg-bearing carbonates. The non-ambiguous detection of carbonate-derived C with LIBS is a challenging issue in which the C signal from the  $\text{CO}_2$  rich atmosphere needs to be differentiated from that of carbonate, which is beyond the scope of the present study.

In summary, the results of the relative line intensity analysis enable the evaluation of variations in the relative intensity of Ca/

Fe, Mg/Fe and Si/Fe at the centimeter scale (regions A, B, C, and D), millimeter scale (X, Y axis), and micrometer scale (Z axis or depth). Thus, our 3D LIBS characterization has revealed: (1) chemical diversity across the surface of the rock sample (four distinct regions analyzed; corroborated by SEM analyses); (2) chemical variation within each of the four regions along the X, Y axis; and (3) chemical variations within each of the four regions as a function of depth (Z axis).

### 3.3. Critical assessment of the methodology

Our data demonstrate the potential of LIBS for not only performing chemical profiles, but for unambiguously detecting layer-to-layer chemical transitions in complex natural geological materials. The ablation and cratering of the substrate by the laser is observed in Fig. 2, where the black basaltic rock is seen through the white coating at the base of the crater. The non-abrupt transition between zones is consistent with previous findings for LIBS analyses of natural rock coatings (e.g., Lanza et al., 2012). This can be explained by a number of factors. First, natural variability and geometric irregularities of the different layers may lead to a diffuse transition between layers. In addition, the material that is being ablated inside the crater and displaced by subsequent shots may not be completely expelled out of the crater. Fine material from previous shots may therefore accumulate inside the craters creating a mixture of material from two (or more) compositionally different layers. Initially, the laser probes only the upper layer. As the laser shot increases, the crater gets deeper and reaches the middle layer, where at the bottom dust from the upper layer can be redeposited into the crater. Eventually, the crater can go deeper

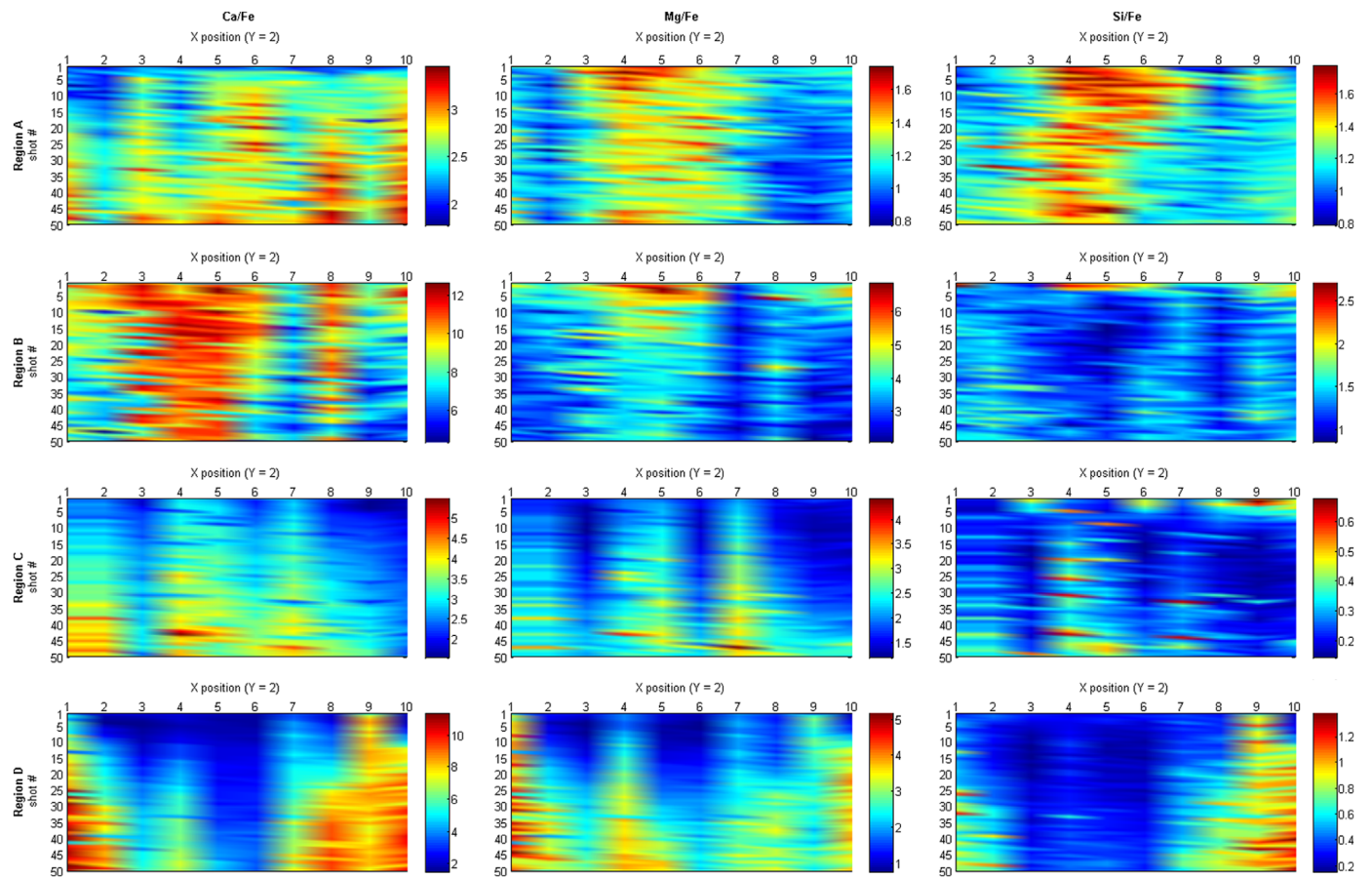


**Fig. 9.** Representation of the lateral and depth variation of the elemental ratios (Ca/Fe, Mg/Fe, Si/Fe). From the matrix of  $X=10$  by  $Y=10$  points analyzed, only a line of points along  $Y=2$  is shown, with 50 laser shots for each  $X$  point.

to reach the lower layer, with an accumulation of material from the middle and upper layers. Also, the crater shape formed by the interaction of the laser pulse with the material is known to be conical (Balzer et al., 2005). Therefore, as the laser shots increase and the crater gets deeper, the plasma plume generated is more susceptible to interact with the walls of the crater, and hence the different layers may all contribute partially to the overall plasma emission (Alm, 2011). Furthermore, the interaction of matter with nanosecond laser pulses can induce melting of the sample causing the modification and mixing of different layers. As a consequence, the depth resolution is adversely affected (Margetic et al., 2001; Alm, 2011). Yet despite these complications, our data demonstrate that mineral coatings on natural rocks or multi-layered fine-scale deposits can be identified by increasing or decreasing trends in elemental ratios, as determined by qualitative LIBS analysis. Such a LIBS coating signature is consistent with previous laboratory work (Lanza et al., 2012) and appears to be consistent with preliminary results from LIBS analyses with the ChemCam instrument on Mars (Blaney et al., 2013; Lanza et al., 2013; Léveillé et al., 2014; Lanza et al., 2015).

#### 3.4. Implications for planetary exploration

The changes in chemical composition with depth in each of the layers can most likely be attributed to differences in mineralogical composition of each layer. As such, these differences record changes in the composition of fluids that have interacted with the rock and deposited mineral coatings. Our results are therefore consistent with multiple episodes of mineral deposition on the basaltic rock substrate. Various carbonate-rich coatings and cements have been

studied at the Sverrefjell and neighboring volcanic complexes (e.g., Treiman et al., 2002; Morris et al., 2010, 2011; Blake et al., 2011). The sample used in our study appears to be most similar to those of Morris et al. (2011). While these studies have noted mainly carbonate-rich coatings, with some indication of iron-oxides (hematite, magnetite; Morris et al., 2011), silica-rich coatings have yet to be described. In our sample, the enrichment in Si observed in the upper portions of regions C and D could be due to Si-substitution in iron-oxides or a distinct opal-like phase mixed with iron-oxides and possibly carbonates. The lower layers, which we interpret to be rich in Ca-Mg-carbonates, are generally consistent with previous studies of coatings and cements from this area, though we cannot rule out the possible presence of Fe-carbonate as detected and reported in other studies (Treiman et al., 2002; Morris et al., 2011; Blake et al., 2011). Our results demonstrate that the fluids evolved from a Ca-Mg-dominant composition to a Fe-Si-dominant composition over some period of time when aqueous activity was most prevalent. This could be a result of changes in fluid temperature due to changes in heat source (volcanic or magmatic activity), or may represent a change in fluid composition due to varying water-rock interactions. The ability to recognize similar past changes in fluid composition on such a small scale is critical during planetary missions in order to assess and quantify past aqueous activity, and ultimately habitability.

We have presented detailed three-dimensional chemical data obtained by LIBS on natural rock coatings. While the depth profiling capability of LIBS is often touted as one of its main advantages, we show that LIBS depth profiles on natural rocks can be challenging to interpret due to the complex interaction between laser, plasma and sample, in addition to natural chemical and textural variability. As

such, the obtained spectra are not straightforward to interpret. Nevertheless, gradual changes in element intensity ratios can be used to recognize the presence of coatings or layers of differing compositions especially when performing depth profiles (e.g., greater than 50 laser shots at a single location). Such a coating signature was also described in Lanza et al. (2015), and it can be valuable in tactical operations of planetary missions, such as by helping to target samples for more detailed in situ study or collection and return to Earth. In particular, the possibility of remotely and rapidly detecting the presence of a coating or of multiple-layers in fine-scale structures (e.g., veins, concretions) could significantly accelerate rover-based operations by triaging a large number of potential targets before utilizing other instruments. For example, the ChemCam instrument on the Curiosity rover can potentially identify coatings or layering at a distance of up to 7 m from the rover, and with a high spatial resolution of less than 1 mm (Wiens et al., 2012; Maurice et al., 2012; Lanza et al., 2012; Lanza et al., 2015). Subsequently, arm-mounted instruments and body-mounted analytical instruments could then be used on prioritized targets. Such a strategy can save time when compared to using an arm-mounted rock abrasion tool and APXS instrument, as done for the MER mission (Knoll et al., 2008), and allows for unprecedented lateral and vertical spatial resolution. Since elucidating past fluid compositions on Mars is one of the key requirements for assessing past habitable conditions, our results show great promise for detecting, identifying and characterizing similar coatings by LIBS on Mars. In particular, the temporal record of interactions between the Martian lithosphere, hydrosphere and atmosphere may be elucidated by careful LIBS analysis of fine-scale features, such as mineral coatings on rocks, multi-layered veins and layered concretions.

#### 4. Conclusions

In this paper, we have demonstrated the capability of LIBS to differentiate complex mineral coatings based on their chemical composition, and even more, to detect layer-to-layer chemical transitions. Our analysis was performed on a subglacial volcanic Martian analog rock from Svalbard, Norway, in Mars-simulated laboratory conditions, in which we observed three-dimensional chemical variations of the main elements present (Ca, Mg, Fe, Si) and corroborated by SEM analysis. The variations in the elemental intensity ratios can be correlated to different mineralogical layers that record changes in the composition of fluids in multiple episodes of mineral deposition. This LIBS signature of coatings is a powerful tool in tactical operations of planetary missions. It can efficiently be used to identify potential targets and determine the chemical composition of layers, providing critical information for further detailed analysis during exploration mission.

#### Acknowledgments

The authors acknowledge the AMASE 2011 Team led by A. Steele and H.E.F. Amundsen for assistance during field activities. CL and PS acknowledge the financial support from the Natural Sciences and Engineering Research Council of Canada (NSERC) and the Canadian Space Agency (CSA). PS acknowledges financial support from the McDonnell Center for Space Sciences at Washington University in St. Louis and from the NASA Mars Fundamental Research Program, Grant #: NNX13AJ18G. ACE acknowledges financial support from the Ministerio de Economía y Competitividad of Spain.

#### References

- Alm, L., 2011. Development of Laser-Induced Breakdown Spectroscopy for Analyzing Rinds and Layered Structures in Martian Rocks (Master thesis). Luleå University of Technology, Luleå, Sweden, pp. 1–82.
- Alvira, F.C., Orzi, D.J.O., Bilmes, G.M., 2009. Surface treatment analyses of car bearings by using laser-induced breakdown spectroscopy. *Appl. Spectrosc.* 63, 192–198.
- Amundsen, H.E.F., Benning, L., Blake, D.F., Fogel, M., Ming, D., Skidmore, M., Steele, A., AMASE Team, 2011. Cryogenic origin for Mars analog carbonates in the bockfjord volcanic complex, Svalbard (Norway) [abstract 2223]. In: Proceedings of the 42nd Lunar and Planetary Institute Science Conference Abstracts. Lunar and Planetary Institute, Houston.
- Balzer, H., Hoehne, M., Sturm, V., Noll, R., 2005. Online coating thickness measurement and depth profiling of zinc coated sheet steel by laser-induced breakdown spectroscopy. *Spectrochim. Acta Part B At. Spectrosc.* 60, 1172–1178.
- Bishop, J.L., Murchie, S.L., Pieters, C.M., Zent, A.P., 2002. A model for formation of dust, soil, and rock coatings on Mars: physical and chemical processes on the Martian surface. *J. Geophys. Res.* 107, 7–1–7–17.
- Blake, D.F., Treiman, A.H., Morris, R., Bish, D., Amundsen, H.E.F., Steele, A., 2011. Carbonate cements from the Sverrefjell and Sigurdjell volcanos, Svalbard Norway: analogs for martian carbonates [abstract 2167]. In: Proceedings of the 42nd Lunar and Planetary Institute Science Conference Abstracts. Lunar and Planetary Institute, Houston.
- Blaney, D.L., Anderson, R., Berger, G., Bridges, J.C., Bridges, N.T., Clark, B., Clegg, S.M., Dyr, M.D., Ehlmann, B.L., Goetz, W., King, P.L., Lanza, N.L., Mangold, N., Meslin, P.-Y., Newsom, H.E., the MSL Science Team, 2013. Assessment of potential rock coatings at rocknest, Gale Crater with ChemCam [abstract 1568]. In: Proceedings of the 44th Lunar and Planetary Institute Science Conference Abstracts. Lunar and Planetary Institute, Houston.
- Cabalín, L.M., Lez, A.G., Lazić, V., Laserna, J., 2011. Deep ablation and depth profiling by laser-induced breakdown spectroscopy (LIBS) employing multi-pulse laser excitation: application to galvanized steel. *Appl. Spectrosc.* 65, 797–805.
- Ciucci, A., Corsi, M., Palleschi, V., Rastelli, S., Salvetti, A., Tognoni, E., 1999. New procedure for quantitative elemental analysis by laser-induced plasma spectroscopy. *Appl. Spectrosc.* 53, 960–964.
- Clegg, S.M., Sklute, E., Dyr, M.D., Barefield, J.E., Wien, R.C., 2009. Multivariate analysis of remote laser-induced breakdown spectroscopy spectra using partial least squares principal component analysis, and related techniques. *Spectrochim. Acta Part B* 64, 79–88.
- Cousin, A., 2012. LIBS (Laser-Induced Breakdown Spectroscopy) pour l'exploration martienne (Doctoral thesis). Université Toulouse 3 Paul Sabatier, Toulouse, France, pp. 1–213.
- Dorn, R.I., 1998. Rock coatings. *Developments in Earth Surface Processes Series*. Elsevier, New York, pp. 1–429.
- Doucet, F.R., Belliveau, T.F., Fortier, J.-L., Hubert, J., 2007. Use of chemometrics and laser-induced breakdown spectroscopy for quantitative analysis of major and minor elements in aluminum alloys. *Appl. Spectrosc.* 61, 327–332.
- Dubey, A., Boukouvala, F., Keyvan, G., Hsia, R., Saranteas, K., Brone, D., Misra, T., Ierapetritou, M.G., Muzzio, F.J., 2012. Improvement of tablet coating uniformity using a quality by design approach. *AAPS PharmSciTech* 13, 231–246.
- Haskin, L.A., et al., 2005. Water alteration of rocks and soils on Mars at the Spirit rover site in Gusev crater. *Nature* 436, 66–69. <http://dx.doi.org/10.1038/nature03640>.
- Kim, T., Nguyen, B.T., Minassian, V., Lin, C.T., 2007. Paints and coatings monitored by laser-induced breakdown spectroscopy. *J. Coat. Technol. Res.* 4, 241–253.
- Koujelev, A., Lui, S.-L., 2011. Artificial neural networks for material identification, mineralogy and analytical geochemistry based on laser-induced breakdown spectroscopy. In: Suzuki, K., (Ed.), *Artificial Neural Networks – Industrial and Control Engineering Applications*. Intech, India, pp. 91–116.
- Knoll, A.H., Jolliff, B.L., Farrand, W.H., Bell, J.F., Clark, B.C., Gellert, R., Golombek, M.P., Grotzinger, J.P., Herkenhoff, K.E., Johnson, J.R., McLennan, S.M., Morris, R., Squyres, S.W., Sullivan, R., Tosca, N.J., Yen, A., Learner, Z., 2008. Veneers, rinds, and fracture fills: relatively late alteration of sedimentary rocks at Meridiani Planum, Mars. *J. Geophys. Res. E: Planets* 113 (E06S16-1–06S16-27).
- Lanza, N.L., Clegg, S.M., Wiens, R.C., McInroy, R.E., Newsom, H.E., Deans, M.D., 2012. Examining natural rock varnish and weathering rinds with laser-induced breakdown spectroscopy for application to ChemCam on Mars. *Appl. Opt.* 51, B74–B82.
- Lanza, N.L., Anderson, R.B., Blaney, D., Bridges, N.T., Clark, B., Clegg, S.M., Delapp, D., Ehlmann, B.L., Hardgrove, C.J., Léveillé, R., Mangold, N., Melikechi, N., Meslin, P.-Y., Mezzacappa, A., Newsom, H.E., Ollila, A., Wiens, R.C., MSL Science Team, 2013. Evidence for rock surface alteration with ChemCam from curiosity's first 90 sols [abstract 1723]. In: Proceedings of the 44th Lunar and Planetary Institute Science Conference Abstracts. Lunar and Planetary Institute, Houston.
- Lanza, N.L., Ollila, A.M., Cousin, A., Wiens, R., Clegg, S., Mangold, N., Bridges, N., Cooper, D., Schmidt, M., Berger, J., Arvidson, R., Melikechi, N., Newsom, H., Tokar, R., Hardgrove, C., Mezzacappa, A., Jackson, R.S., Clark, B., Forni, O., Maurice, S., Nachon, M., Anderson, R.B., Blank, J., Deans, M., Delapp, D., Léveillé, R., McInroy, R., Martinez, R., Meslin, P.-Y., Pinet, P., 2015. Understanding the signature of rock coatings in laser-induced breakdown spectroscopy data. *Icarus* 249, 62–73.
- Léveillé, R., Wiens, R.C., Anderson, R.B., Berger, G., Bridges, J., Clark, B., Cousin, A., Edgar, L., Fabre, C., Forni, O., Grotzinger, J., Kah, J., Lanza, N., Lasue, J., Le Mouelic, S., Leshin, L., Mangold, N., Maurice, S., McLennan, S., Meslin, P.-Y., Mezzacappa, Newsom, H., Ollila, A., Siebach, K., 2014. ChemCam investigation of resistant

- fracture-fill cements at yellowknife Bay, Gale Crater, Mars. *J. Geophys. Res. - Planets*, 2014. <http://dx.doi.org/10.1002/2014JE004620>.
- Madamba, M.C., Mullett, W.M., Debnath, S., Kwong, E., 2007. Characterization of tablet film coatings using a laser-induced breakdown spectroscopic technique. *AAPS PharmSciTech* 8, 184–190.
- Mahaney, W.C., Fairén, A.G., Dohm, J.M., Krinsley, D.H., 2012. Weathering rinds on clasts: examples from Earth and Mars as short and long term recorders of paleoenvironment. *Planet. Space Sci.* 73, 243–253.
- Margetic, V., Bolshov, M., Stockhaus, A., Niemax, K., Hergenröder, R., 2001. Depth profiling of multi-layer samples using femtosecond laser ablation. *J. Anal. At. Spectrom.* 16, 616–621.
- Maurice, S., Wiens, R.C., Saccoccia, M., Barracough, B., Gasnault, O., Forni, O., Mangold, N., Baratoux, D., Bender, S., Berger, G., Bernardin, J., Berthé, M., Bridges, N., Blaney, D., Bouyé, M., Caïs, P., Clark, B., Clegg, S., Cousin, A., Cremers, D., Cros, A., DeFlores, L., Derycke, C., Dingler, B., Dromart, G., Dubois, B., Dupieux, M., Durand, E., d'Uston, L., Fabre, C., Faure, B., Gaboriaud, A., Gharsa, T., Herkenhoff, K., Kan, E., Kirkland, L., Kouach, D., Lacour, J.-L., Langevin, Y., Lasue, J., Le Mouélic, S., Lescure, M., Lewin, E., Limonadi, D., Manhes, G., Mauchien, P., McKay, C., Meslin, P.-Y., Michel, Y., Miller, E., Newsom, H.E., Ortner, G., Paillet, A., Parès, L., Parot, Y., Pérez, R., Pinet, P., Poitrasson, F., Quertier, B., Sallé, B., Sotin, C., Sautter, V., Séran, H., Simmonds, J.J., Sirven, J.-B., Stiglich, R., Striebig, N., Thocaven, J.-J., Toplis, M.J., Vaniman, D., 2012. The ChemCam instrument suite on the Mars Science Laboratory (MSL) rover: science objectives and mast unit description. *Space Sci. Rev.* 170, 95–166.
- McSween, H.Y., Wyatt, M.B., Gellert, R., Bell, J.F., Morris, R.V., Herkenhoff, K.E., Crumpler, L.S., Milam, K.A., Stockstill, K.R., Tornabene, L.L., Arvidson, R.E., Bartlett, P., Blaney, D., Cabrol, N.A., Christensen, P.R., Clark, B.C., Crisp, J.A., Des Marais, D.J., Economou, T., Farmer, J.D., Farrand, W., Ghosh, A., Golombek, M., Gorevan, S., Greeley, R., Hamilton, V.E., Johnson, J.R., Joliff, B.L., Klingelhöfer, G., Knudson, A.T., McLennan, S., Ming, D., Moersch, J.E., Rieder, R., Ruff, S.W., Schröder, C., de Souza Jr., P.A., Squyres, S.W., Wänke, H., Wang, A., Yen, A., Zipf, J., 2006. Characterization and petrologic interpretation of olivine-rich basalts at Gusev Crater, Mars. *J. Geophys. Res. Planets* 111 (E02S10-1-E02S10-17).
- Michalski, J.R., Kraft, M.D., Sharp, T.G., Christensen, P.R., 2006. Effects of chemical weathering on infrared spectra of Columbia River Basalt and spectral interpretations of martian alteration. *Earth Planet. Sci. Lett.* 248, 822–829.
- Morris, R.V., Ruff, S.W., Gellert, R., Ming, D.W., Arvidson, R.E., Clark, B.C., Golden, D.C., Siebach, K., Klingelhöfer, G., Schröder, C., Fleischer, I., Yen, A.S., Squyres, S.W., 2010. Identification of carbonate-rich outcrops on Mars by the Spirit rover. *Science* 329, 421–424.
- Morris, R.V., Blake, D.F., Bish, D., Ming, D.W., Agresti, D.G., Treiman, A.H., Steele, A., Amundsen, H.E.F., 2011. A terrestrial analogue from Spitsbergen (Svalbard, Norway) for the comanche carbonate at Gusev Crater, Mars [abstract 1699]. In: Proceedings of the 42nd Lunar and Planetary Institute Science Conference Abstracts. Lunar and Planetary Institute, Houston.
- Niles, P.B., Catling, D.C., Berger, G., Chassefière, E., Ehlmann, B.L., Michalski, J.R., Morris, R., Ruff, S.W., Sutter, B., 2013. Geochemistry of carbonates on Mars: implications for climate history and nature of aqueous environments. *Space Sci. Rev.* 174, 301–328.
- Noll, R., 2012. Laser-Induced Breakdown Spectroscopy: Fundamentals and Application. Springer, Berlin, Heidelberg (pp. 1–453).
- Novotný, K., Vaculovič, T., Galiová, M., Otruba, V., Kanický, V., Kaiser, J., Liška, M., Samek, O., Malina, R., Páleníková, K., 2007. The use of zinc and iron emission lines in the depth profile analysis of zinc-coated steel. *Appl. Surf. Sci.* 253, 3834–3842.
- Salvatore, M.R., Mustard, J.F., Head, J.W., Cooper, R.F., Marchant, D.R., Wyatt, M.B., 2013. Development of alteration rinds by oxidative weathering processes in Beacon Valley, Antarctica, and implications for Mars. *Geochim. Cosmochim. Acta* 115, 137–161.
- Sharma, S.K., Misra, A.K., Lucey, P.G., Wiens, R.C., Clegg, S.M., 2007. Combined remote LIBS and Raman spectroscopy at 8.6 m of sulfur-containing minerals, and minerals coated with hematite or covered with basaltic dust. *Spectrochim. Acta Part A* 68, 1036–1045.
- Sirven, J.-B., Sallé, B., Mauchien, P., Lacour, J.-L., Maurice, S., Manthès, G., 2007. Feasibility study of rock identification at the surface of Mars by remote laser-induced breakdown spectroscopy and three chemometric methods. *J. Anal. At. Spectrom.* 22, 1471–1480.
- Skjelkvåle, B.L., Amundsen, H.E.F., O'Reilly, S.Y., Griffin, W.L., Gjelsvik, T., 1989. A primitive alkali basaltic stratovolcano and associated eruptive centres, northwestern Spitsbergen: volcanology and tectonic significance. *J. Volcanol. Geotherm. Res.* 37, 1–19.
- Sobron, P., Lefebvre, C., Léveillé, R., Koujelev, A., Haltigin, T., Du, H., Wang, A., Cabrol, N., Zacny, K., Craft, J., 2013. Geochemical profile of a layered outcrop in the Atacama analogue using laser-induced breakdown spectroscopy (LIBS) – implications for curiosity investigations in Gale. *Geophys. Res. Lett.* 40, 1965–1970.
- Steele, A., Amundsen, H.E.F., Teams, A., 2011. Svalbard as a Mars analogue site and the Arctic Mars Analogue Svalbard Expedition (AMASE) analogue sites [abstract 6041]. In: Analogue Sites for Mars Missions: MSL and Beyond Conference Abstracts. Lunar and Planetary Institute, Houston.
- St-Onge, L., Sabsabi, M., 2000. Towards quantitative depth-profile analysis using laser-induced plasma spectroscopy: investigation of galvannealed coatings on steel. *Spectrochim. Acta Part B* 55, 299–308.
- Treiman, A.H., Amundsen, H.E., Blake, D.F., Bunch, T., 2002. Hydrothermal origin for carbonate globules in Martian meteorite ALH84001: a terrestrial analogue from Spitsbergen (Norway). *Earth Planet. Sci. Lett.* 204, 323–332.
- Vadillo, J.M., Laserna, J.J., 1997. Depth-resolved analysis of multilayered samples by laser-induced breakdown spectrometry. *J. Anal. At. Spectrom.* 12, 859–862.
- Wiens, R.C., Kirkland, L.E., McKay, C.P., Cremers, D.A., Thompson, J., Maurice, S., Pinet, P.C., 2004. Analyses of IR-stealthy and coated surface materials: a comparison of LIBS and reflectance spectra and their application to Mars surface exploration [abstract 1695]. In: Proceedings of the 35th Lunar and Planetary Institute Science Conference Abstracts. Lunar and Planetary Institute, Houston.
- Wiens, C.R., Maurice, S., Barracough, B., Saccoccia, M., Barkley, W.C., Bell III, J.F., Bender, S., Bernardin, J., Blaney, D., Blank, J., Bouyé, M., Bridges, N., Bultman, N., Caïs, P., Clanton, R.C., Clark, B., Clegg, S., Cousin, A., Cremers, D., Cros, A., DeFlores, L., Delapp, D., Dingler, R., d'Uston, C., Dyar, M.D., Elliott, T., Enemark, D., Fabre, C., Flores, M., Forni, O., Gasnault, O., Hale, T., Hays, C., Herkenhoff, K., Kan, E., Kirkland, L., Kouach, D., Landis, D., Langevin, Y., Lanza, N., LaRocca, F., Lasue, J., Latino, J., Limonadi, D., Lindensmith, C., Little, C., Mangold, N., Manhes, G., Mauchien, P., McKay, C., Miller, E., Mooney, J., Morris, R.V., Morrison, L., Nelson, T., Newsom, H., Ollila, A., Ott, M., Pares, L., Perez, R., Poitrasson, F., Provost, C., Reiter, J.W., Roberts, T., Romero, F., Sautter, V., Salazar, S., Simmonds, J.J., Stiglich, R., Storms, S., Striebig, N., Thocaven, J.-J., Trujillo, T., Ulibarri, M., Vaniman, D., Warner, N., Waterbury, R., Whitaker, R., Witt, J., Wong-Swanson, B., 2012. The ChemCam instrument suite on the Mars Science Laboratory (MSL) rover: body unit and combined system tests. *Space Sci. Rev.* 170, 167–227.